Relaxation Oscillations, Stability, and Cavity Feedback in a Superradiant Raman Laser

Justin G. Bohnet,* Zilong Chen, Joshua M. Weiner, Kevin C. Cox, and James K. Thompson
JILA, NIST and Department of Physics, University of Colorado, Boulder, Colorado 80309-0440, USA
(Received 30 August 2012; published 18 December 2012)

We experimentally study the relaxation oscillations and amplitude stability properties of an optical laser operating deep into the bad-cavity regime using a laser-cooled ^{87}Rb Raman laser. By combining measurements of the laser light field with nondemolition measurements of the atomic populations, we infer the response of the gain medium represented by a collective atomic Bloch vector. The results are qualitatively explained with a simple model. Measurements and theory are extended to include the effect of intermediate repumping states on the closed-loop stability of the oscillator and the role of cavity feedback on stabilizing or enhancing relaxation oscillations. This experimental study of the stability of an optical laser operating deep into the bad-cavity regime will guide future development of superradiant lasers with ultranarrow linewidths.

DOI: 10.1103/PhysRevLett.109.253602 PACS numbers: 42.55.Ye, 42.50.Nn, 42.50.Pq, 42.60.Rn

Optical lasers operating deep in the bad-cavity or superradiant regime, in which the cavity linewidth κ is much larger than the gain bandwidth $\gamma_\perp$, have attracted recent theoretical [1,2] and experimental [3–5] interest. The interest has been partially driven by the possibility of creating spectrally narrow lasers with linewidths ≤ 1 mHz and dramatically reduced sensitivity to the vibrations that limit state of the art narrow lasers and keep them from operating outside the laboratory environment [6]. These lasers may improve measurements of time [7], gravity [8], and fundamental constants [9,10] aiding the search for physics beyond the standard model. The cold-atom Raman superradiant laser utilized here operates deep into the bad-cavity regime ($\kappa/\gamma_\perp \approx 10^3 \gg 1$), making it an important physics test bed for fundamental and practical explorations of bad-cavity optical lasers.

In the interest of fundamental science and in light of the potential applications, it is important to understand the impact of external perturbations on lasers operating deep into the bad cavity regime. In this Letter, we present an experimental study of the response to external perturbations of the amplitude, atomic inversion, and atomic polarization of an optical laser operating deep into the bad-cavity regime. In contrast, experiments have extensively studied the amplitude stability properties of good-cavity lasers ($\kappa \ll \gamma_\perp$) (see Ref. [11] and references therein). Previous experimental work in the extreme bad-cavity [3] and cross-over regime [12] focused on the phase properties of the light and atomic medium. Amplitude oscillations, intensity noise, and chaotic instabilities have been observed in gas lasers operating near the cross-over regime ($\kappa/\gamma_\perp \leq 10$) [13–16]. Relaxation oscillations of the field have been studied deep into the bad-cavity regime using masers [17] in which the radiation wavelength is comparable to the size of the gain medium, unlike in the present optical system. Previous theoretical studies of amplitude stability deep in the bad-cavity regime include studies of relaxation oscillations [18], chaotic instabilities [19], and intensity fluctuations characterized by correlation functions [18,20].

In good-cavity optical lasers, the atomic polarization (proportional to $J_\perp$) can be adiabatically eliminated and the relaxation oscillations are associated with the flow of energy back and forth between the gain inversion (proportional to J_z) and the cavity field A, where J_z, $J_\perp$ are components of the collective Bloch vector $\vec{J}$ describing the atomic gain medium. In contrast, in a bad-cavity laser, the cavity field can be adiabatically eliminated, and the oscillations are driven by the coupling of $J_\perp$ and J_z. Here, we will measure and infer not only the light field $A(t)$, but also the atomic degrees of freedom $J_\perp(t)$ and $J_z(t)$ using nondemolition cavity-aided measurements [21,22] to give the complete picture of the dynamics of relaxation oscillations in a bad-cavity laser.

We will also consider the effects on the laser's amplitude stability of nonideal repumping through multiple intermediate states. Intermediate repumping states were not included in previous simple theoretical models [1], but are present in most actual realizations. In addition, we demonstrate that the cavity frequency tuning in response to the distribution of atomic population among various ground states can be used to suppress or enhance relaxation oscillations in the Raman transition configuration or other configurations with atomic transitions near-detuned from the lasing mode. As evidence, we show stabilization of J_z, $J_\perp$, and A similar to observations of the suppression of relaxation oscillations in good-cavity lasers [23]. The cavity frequency tuning mechanism is related to other applications of cavity feedback including the creation of nonlinearities for generating spin-squeezed atomic ensembles [24], cavity cooling and amplification in atomic and opto-mechanical systems [25], and the control of instabilities in gravitational wave detectors [26].

Our experimental system consists of a quasi-steady-state Raman laser described in Fig. 1 and in Ref. [3]. The laser

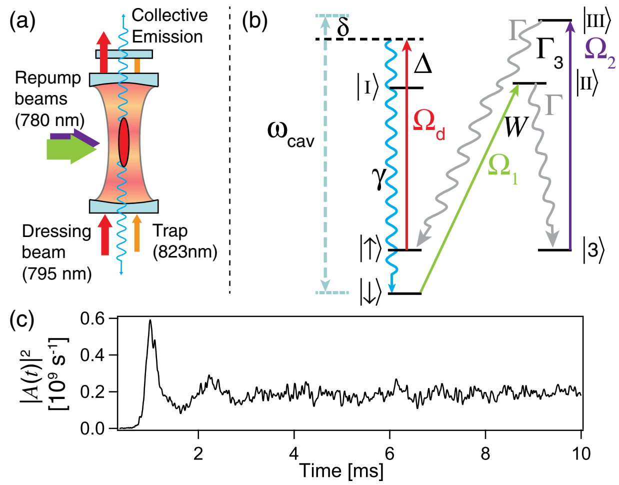

FIG. 1 (color online). (a), (b) Physical setup and energy level diagram. The trapping light and Raman dressing laser (power $\propto \Omega_d^2$) are injected along the cavity axis. The repumping light is applied perpendicular to the cavity axis. The emitted optical laser light is nearly resonant with the cavity mode (dashed lines) detuned from $\omega_{\rm cav}$ by δ. The repumping is accomplished through a pair of two-photon transitions through intermediate optically excited states $|{\rm II}\rangle$ and $|{\rm III}\rangle$ with incoherent decay rates Γ. We individually control the two-photon rates W and Γ_3 with the repumping laser powers $\propto \Omega_{1,2}^2$. $|3\rangle$ represents other metastable ground states besides the laser levels. (c) Example emitted laser photon flux $|A(t)|^2$ versus time showing spiking and relaxation oscillations at turn-on.

uses $N = 1 \times 10^6$ to 2×10^6 ^{87}Rb atoms as the gain medium. The atoms are trapped and laser cooled into the Doppler-insensitive Lamb-Dicke regime (40 μK) in a 1D optical lattice at 823 nm formed by a standing wave in a moderate finesse $F \approx 700$ optical cavity with a cavity power decay rate $\kappa/2\pi = 11$ MHz. The single-atom cavity cooperativity parameter is $C = 8 \times 10^{-3} \ll 1$ and is equivalent to the Purcell factor [27].

Figure 1(b) shows a simplified energy level diagram of a three level Raman laser system. The lasing transition is a spontaneous optical Raman transition with single-particle rate γ from $|\uparrow\rangle \equiv |5^2S_{1/2}F = 2, m_F = 0\rangle$ to $|\downarrow\rangle \equiv |5^2S_{1/2}F = 1, m_F = 0\rangle$. The decay is induced by a 795 nm dressing laser injected into the cavity nonresonantly and detuned from the $|\uparrow\rangle$ to $|{\rm I}\rangle \equiv |5^2P_{1/2}F' = 2\rangle$ transition by $\Delta/2\pi = +1.1$ GHz. The atoms are incoherently repumped back to $|\uparrow\rangle$ in two steps: from $|\downarrow\rangle$ to $|3\rangle$ and then from $|3\rangle$ to $|\uparrow\rangle$, at single-particle rates W and Γ_3, respectively. The third metastable ground state $|3\rangle$ here represents the sum of all other hyperfine ground states in ^{87}Rb. The full energy level diagram with details of the dressing and repumping lasers is provided in Ref. [28].

We control γ (typical value 60 s^{-1}) using the intensity of the dressing laser. We control the repumping rates W and Γ_3 using two 780 nm repumping lasers tuned near resonance with the $|5^2S_{1/2}F = 1, 2\rangle \rightarrow |5^2P_{3/2}F' = 2\rangle$ transitions. The repumping intensities are independently controlled allowing us to set the proportionality factor $r \equiv \Gamma_3/W$. In our experiments, W ranges from 10^3 to 10^5 s^{-1}, and r ranges from 0.01 to 2. The repumping dominates all other homogenous broadening of the $|\uparrow\rangle$ to $|\downarrow\rangle$ transition such that $\gamma_\perp \approx W/2$. The inhomogenous broadening of the transition is $\gamma_{\rm in} \approx 10^3$ s^{-1}. To summarize, the relevant hierarchy of rates characterizing our system is $\kappa \gg \gamma_\perp \approx W/2 \sim NC\gamma > \gamma_{\rm in} \gg \gamma$. The rate $NC\gamma$ sets the scale for the single-particle, collectively enhanced decay rate from $|\uparrow\rangle$ to $|\downarrow\rangle$. Coupling to other transverse and longitudinal cavity modes is negligible.

The frequency of the superradiantly emitted light ω_γ is set by the frequency of the dressing laser and the hyperfine splitting $\omega_{\rm HF}/2\pi = 6.834$ GHz. The detuning of light and cavity resonance frequency is $\delta = 2(\omega_{\rm cav} - \omega_\gamma)/\kappa$, normalized to the cavity half linewidth. The single particle scattering rate from the dressing laser into the cavity mode is $\Gamma_c(\delta) = C\gamma/(1 + \delta^2)$.

The cavity frequency is dispersively tuned by the atomic ensemble $\omega_{\rm cav} = \omega_{\rm bcav} + \sum_k \alpha_k N_k$, where $\omega_{\rm bcav}$ is the bare cavity frequency and α_k is the cavity frequency shift for a single atom in the kth ground Zeeman state resulting from dispersive phase shifts of the intracavity light field.

Since the cavity frequency shift from atoms in the $F = 1, 2$ hyperfine states are not equal, the cavity frequency can provide a measurement of the atomic populations. We can suddenly switch off the repumping and dressing lasers to effectively freeze the atomic populations [4]. We then combine repeated nondemolition cavity frequency measurements [21,22,29,30] and NMR-like rotations [31] to determine $J_z(t) = \langle \frac{1}{2} \sum_{i=1}^N (|\uparrow_i\rangle\langle\uparrow_i| - |\downarrow_i\rangle\langle\downarrow_i|)\rangle$ and $\delta(t)$ [28]. We measure the amplitude of the light field emitted from the cavity $A(t)$ in heterodyne just prior to freezing the system, and along with the measurement of the cavity frequency detuning δ, this provides an inferred value of $J_\perp = |\langle \hat{J}_- \rangle|$ using the relation $A(t) = \sqrt{\Gamma_c(\delta(t))} J_\perp(t)$, where $\hat{J}_- = \sum_{i=1}^N |\downarrow_i\rangle\langle\uparrow_i|$.

We observe characteristic laser spiking and relaxation oscillation behavior in $|A(t)|^2$ as the laser turns on and settles to steady state [Fig. 1(c)]. To systematically study small amplitude deviations about the steady-state values $\bar{J}_z$, $\bar{A}$, and $\bar{J}_\perp$, we apply a swept sine technique, similar to Ref. [32]. We apply a simultaneous small amplitude modulation of the repumping rates as $W(t) = \overline{W}(1 + \epsilon {\rm Re}[e^{i\omega t}])$ and $\Gamma_3(t) = rW(t)$. The modulation frequency ω is scanned over frequencies of order $\overline{W}$, such that $\gamma < \omega \ll \kappa$. We then measure and infer the quantities $A(t)$, $J_\perp(t)$, and $J_z(t)$ as described earlier.

To calculate the transfer function of the applied modulation, the measured light field amplitude $A(t)$ exiting the cavity as a function of time is fit to $A(t) = \bar{A}[1 + a(\omega) \times \cos(\omega t + \phi_a(\omega))]$. The normalized fractional amplitude response transfer function is $T_A(\omega) \equiv a(\omega)/\epsilon$ and the phase response transfer function is $T_\phi \equiv \phi_a(\omega)$. We also define the modulation frequency that maximizes $T_A(\omega)$ as the resonance frequency $\omega_{\rm res}$.

We present the measured transfer functions and atomic responses in Figs. 2–4, with theoretical predictions from a full model for ^{87}Rb for quantitative comparison. To guide the interpretation of the measurements, we present an analogous three-level model for the system shown in Fig. 1(b) that captures qualitative features of the full model [28]. The three-level model uses semiclassical optical Bloch equations to describe the lasing transition and the repumping process. Since $\kappa \gg W, \gamma$, the cavity field can be adiabatically eliminated from the system of equations. Additionally, we have adiabatically eliminated the populations in the optically excited states $|{\rm I}\rangle$, $|{\rm II}\rangle$, $|{\rm III}\rangle$, arriving at the steady state solutions for the inversion $\bar{J}_z$ and collective atomic coherence $\bar{J}_\perp$ [1,33]. The steady state amplitude $\bar{A}$ is maximized at $W = W_{\rm pk} = \frac{1}{2}N\Gamma_c(\bar{\delta})$ where $\bar{\delta}$ is the steady state cavity detuning.

To predict relaxation oscillations and damping, we do a straightforward expansion about the steady state values $\bar{J}_z$, $\bar{J}_\perp$, and $\bar{N}_3$ as $J_z(t) \approx \bar{J}_z(1 + {\rm Re}[j_z(t)])$, $J_\perp(t) \approx \bar{J}_\perp(1 + {\rm Re}[j_\perp(t)])$, and $N_3 \approx \bar{N}_3(1 + {\rm Re}[n_3(t)])$ and ignore terms that are second order in small complex quantities $j_\perp$, j_z, n_3 and repumping modulation amplitude ϵ [18,28,34]. The coupled quadratures j_z and $j_\perp$ respond like the two coupled quadratures of a harmonic oscillator, slightly modified by the presence of the intermediate repumping state $|3\rangle$. In the limit of ideal repumping ($r \to \infty$) as is considered in Ref. [1], we can recast the equations as two uncoupled, second order differential equations

$$\ddot{j}_{z,\perp} + 2\gamma_0 \dot{j}_{z,\perp} + \omega_0^2 j_{z,\perp} = D_{z,\perp}(\omega)\epsilon e^{i\omega t}. \quad (1)$$

When $\bar{\delta} = 0$, the damping rate $\gamma_0 = \overline{W}/2$ is set by the damping of the transverse component $j_\perp$ caused by single-particle wave function collapse associated with the repumping. The natural frequency $\omega_0 = \sqrt{\overline{W}(NC\gamma - \overline{W})} = \sqrt{2}\bar{J}_\perp C\gamma$ is set by the steady-state rate of converting collective transverse coherence into inversion $\bar{J}_\perp^2 C\gamma$, normalized by the total steady state coherence $\bar{J}_\perp$.

The responses of the two quadratures to the modulation are different because the effective drives are different with $D_\perp(\omega) = \frac{\overline{W}}{2}(NC\gamma - 2\overline{W} - i\omega)$ and $D_z(\omega) = (NC\gamma - \overline{W})\times(\overline{W} + i\omega)$. Note that the magnitude and phase of the drives change with the modulation frequency and repumping rate, even as the modulation depth ϵ remains constant.

We show this driven oscillator response in Fig. 2(a) with the measured and predicted parametric plot of J_z and $J_\perp$ at three different applied modulation frequencies, with repumping near $\overline{W} = W_{\rm pk}$. Although the characteristic frequencies and rates of the atomic oscillator do not change, the differing drives lead to a change in the phase relationship between the response of the two quadratures. We believe the discrepancy with theory in the center panel of Fig. 2(a) is the beginning of nonlinearity in the system as

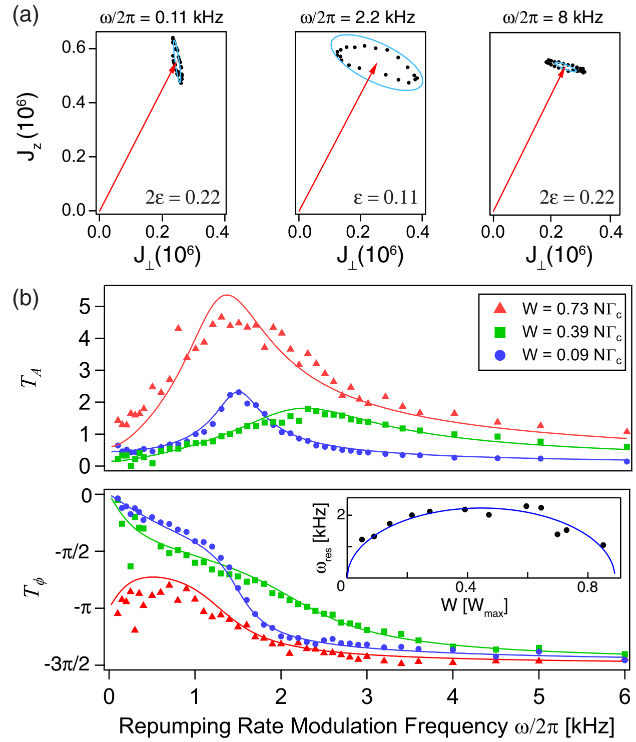

FIG. 2 (color online). (a) Parametric plots of the Bloch vector components $J_z(t)$ and $J_\perp(t)$ over a single cycle of modulation of the repumping rate for modulation frequencies below, near, and above resonance or $\omega/2\pi = 0.11$, 2.2, 8 kHz, from left to right. The points are the measured small-signal deviations about the measured steady-state Bloch vector (arrow). The solid curve is the predicted deviation from steady-state given the experimental parameters $N = 1.3 \times 10^6$, $r = 0.71$, $\bar{\delta} = 1$, $\overline{W} = 0.35NC\gamma$, and $NC\gamma = 125 \times 10^3\ {\rm s}^{-1}$. The modulation depth ϵ for data below and above resonance was doubled to make the response more visible. (b) The amplitude (upper) and phase (lower) response transfer functions $T_A(\omega)$, $T_\phi(\omega)$ of the light field for three values of the repumping rate W. The points are measured data, and the lines are zero free-parameter predictions of the response. (Inset) $\omega_{\rm res}$ versus W (points) and a fit to ω_0 (line) showing the expected frequency dependence of the relaxation oscillations on repumping rate.

it responds beyond the small perturbation regime near resonance.

In Fig. 2(b), we focus on the light field's transfer functions $T_{\rm A}(\omega)$ and $T_\phi(\omega)$. Data for three different average repumping rates $\bar{W}$ are shown. The data display the features of the simple three-level model, namely, increased damping with $\overline{W}$, ω_0 scaling with $\overline{W}$ (inset), the 270° phase shift of T_ϕ at high modulation frequencies, the small response near $\omega = 0$ and $\overline{W} = W_{\rm pk}$ caused by the cancellation in the drive term $D_\perp(\omega)$, and finally the phase reversal of the response near $\omega = 0$ going from below to above $W_{\rm pk}$. The data also quantitatively agree with the displayed theory calculated for the full model including all ^{87}Rb levels. We suspect the deviation for $\overline{W} = 0.73N\Gamma_c$ is a result of a systematic error in measuring the total atom number.

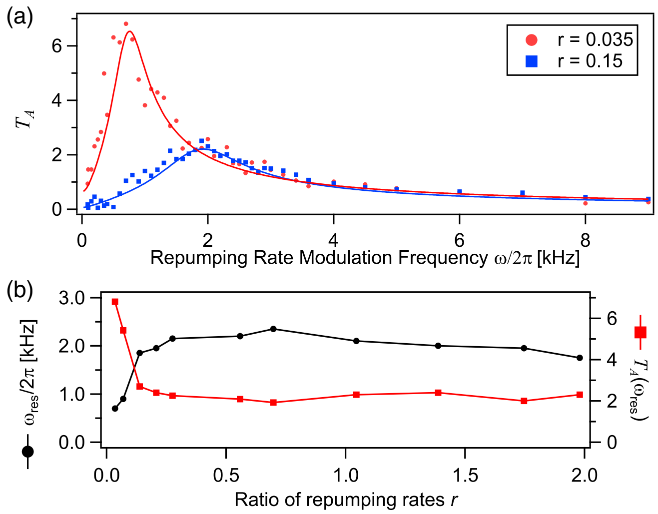

FIG. 3 (color online). Effects of finite ratio of repumping rate r (a) Comparison at two values of r of $T_A(\omega)$ versus modulation frequency. The points are measured data in good agreement with the zero-free parameter fit (lines). (b) Plot of the resonance frequency ω_{res} (circle) and the peak value $T_A(\omega_{\text{res}})$ (square) versus r.

In this work, the repumping ratio $r \neq \infty$, and the theory must be extended to quantitatively describe the data. The physical effect of finite r is that population builds up in $|3\rangle$. The ratio of steady state populations is simply $\bar{N}_3/\bar{N}_\downarrow = 1/r$. As a result of a non-negligible $\bar{N}_3$, the natural frequency is slightly modified as $\omega_0 = \sqrt{\frac{r}{1+r}\overline{W}(NC\gamma - \overline{W})}$. The effective damping in the presence of a harmonic drive at frequency ω is $\gamma_0 = \frac{\overline{W}}{2}\frac{r^2}{(1+r)(1/2+r)} + \frac{r(NC\gamma-\overline{W})}{2(1+r)(1/2+r)} - \frac{\omega^2}{\overline{W}(1+r)}$. The frequency dependent term results from the additional phase shift introduced into the oscillating system as a result of time spent in $|3\rangle$. Despite the frequency-dependent reduction of the damping, as long as $\gamma_0 > 0$ near $\omega = \omega_0$, the system will remain stable. We can experimentally observe a reduction in damping as $r \to 0$, shown in Fig. 3. From the form of ω_0 and γ_0, we expect to see the resonance frequency sharply decrease, and an increase in the peak relaxation oscillation amplitude, as $r \to 0$, which we observe in Fig. 3(b).

To understand the dynamic tuning of the cavity resonance frequency ω_{cav} in response to changes in the atomic populations, we consider the case $r \to \infty$ and $\bar{\delta} \neq 0$. We also assume the cavity frequency is tuned by the atomic inversion J_z as $\alpha = \alpha_\downarrow = -\alpha_\uparrow > 0$. The dynamic cavity tuning then modifies the damping rate as $\gamma_0 = \frac{\overline{W}}{2}(1 + 2\alpha\bar{\delta}(\frac{N}{1+\bar{\delta}^2} - \frac{\overline{W}}{C\gamma}))$. The dispersive tuning of the cavity frequency can act as either positive or negative feedback on the oscillations of $J_{\perp,z}$ for $\bar{\delta} < 0$ and >0, respectively. As an example, in the case of negative feedback, if the inversion J_z decreases, the cavity tunes away from resonance with the Raman transition, reducing the superradiant

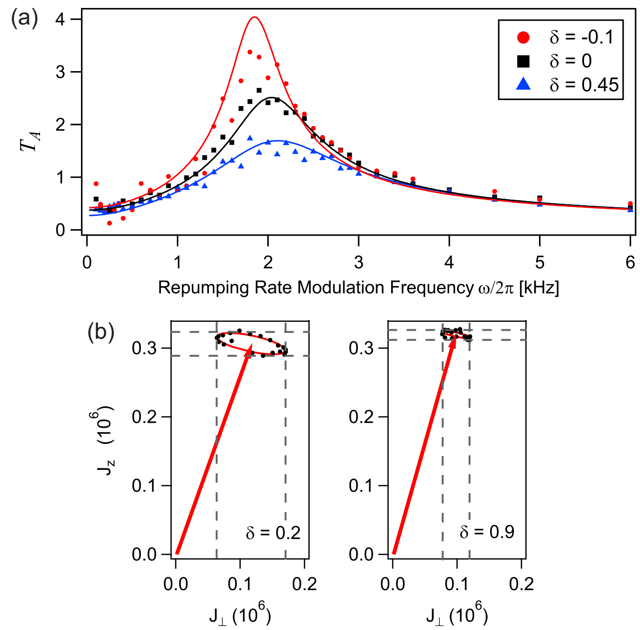

FIG. 4 (color online). Evidence of negative and positive cavity feedback. (a) Amplitude transfer functions of the emitted electric field for three detunings from cavity resonance. The data points are the average of 4 experimental trials. The lines are fitted transfer functions with N as a free parameter. (b) Cavity damping of collective atomic degrees of freedom. The response going from $\bar{\delta} = 0.2$ (left) where the γ_0 is small to $\bar{\delta} = 0.9$ (right) where the system is expected to be critically damped. The solid curves are sinusoidal fits to the data (circles). The dashed lines highlight the damping in both $J_\perp$ and J_z.

emission from $|\uparrow\rangle$ to $|\downarrow\rangle$, and allowing the repumping to restore the inversion more quickly. We observe both positive and negative feedback in the measured transfer function $T_A(\omega)$ and the atomic responses $J_z(t)$ and $J_\perp(t)$ as shown in Fig. 4.

We have studied the dynamics of the polarization, inversion, and field of an optical laser operating deep in the bad-cavity regime. We have shown that dispersive cavity frequency tuning can suppress or enhance relaxation oscillations. Having experimentally validated our model for optical lasers in the extreme bad-cavity regime, future work can now extend the formalism to realistic models of proposed ultrastable lasers using ultranarrow atomic transitions in atoms such as Sr and Yb [1]. In the future, it should be possible to directly monitor $J_\perp$ using techniques similar to those presented here to monitor J_z. Further studies of the nonlinear dynamics of the extreme bad-cavity laser system will include investigations of chaos [19] and squeezed light generation [35].

The authors acknowledge helpful discussions with D. Meiser, M. J. Holland, J. Ye, D. Z. Anderson, and S. T. Cundiff. This work was funded by NSF PFC, NIST, ARO, and DARPA QuASAR. J. G. B. acknowledges support from NSF GRF, and Z. C. acknowledges support from A*STAR Singapore.

*To whom all correspondence should be addressed. bohnet@jilau1.colorado.edu

[1] D. Meiser, J. Ye, D. R. Carlson, and M. J. Holland, Phys. Rev. Lett. **102**, 163601 (2009).
[2] J. Chen, Chin. Sci. Bull. **54**, 348 (2009).
[3] J. G. Bohnet, Z. Chen, J. M. Weiner, D. Meiser, M. J. Holland, and J. K. Thompson, Nature (London) **484**, 78 (2012).
[4] J. G. Bohnet, Z. Chen, J. W. Weiner, K. C. Cox, and J. K. Thompson, arXiv:1208.1710v2.
[5] J. W. Weiner, K. C. Cox, J. G. Bohnet, Z. Chen, and J. K. Thompson, arXiv:1210.3663.
[6] Y. Y. Jiang, A. D. Ludlow, N. D. Lemke, R. W. Fox, J. A. Sherman, L.-S. Ma, and C. W. Oates, Nat. Photonics **5**, 158 (2011).
[7] A. D. Ludlow, T. Zelevinsky, G. K. Campbell, S. Blatt, M. M. Boyd, M. H. G. de Miranda, M. J. Martin, J. W. Thomsen, S. M. Foreman, J. Ye, T. M. Fortier, J. E. Stalnaker, S. A. Diddams, Y. L. Coq, Z. W. Barber, N. Poli, N. D. Lemke, K. M. Beck, and C. W. Oates, Science **319**, 1805 (2008).
[8] C. W. Chou, D. B. Hume, T. Rosenband, and D. J. Wineland, Science **329**, 1630 (2010).
[9] T. M. Fortier, N. Ashby, J. C. Bergquist, M. J. Delaney, S. A. Diddams, T. P. Heavner, L. Hollberg, W. M. Itano, S. R. Jefferts, K. Kim, F. Levi, L. Lorini, W. H. Oskay, T. E. Parker, J. Shirley, and J. E. Stalnaker, Phys. Rev. Lett. **98**, 070801 (2007).
[10] S. Blatt, A. D. Ludlow, G. K. Campbell, J. W. Thomsen, T. Zelevinsky, M. M. Boyd, J. Ye, X. Baillard, M. Fouché, R. L. Targat, A. Brusch, P. Lemonde, M. Takamoto, F.-L. Hong, H. Katori, and V. V. Flambaum, Phys. Rev. Lett. **100**, 140801 (2008).
[11] D. E. McCumber, Phys. Rev. **141**, 306 (1966).
[12] S. J. M. Kuppens, M. P. van Exter, and J. P. Woerdman, Phys. Rev. Lett. **72**, 3815 (1994).
[13] L. Casperson, IEEE J. Quantum Electron. **14**, 756 (1978).
[14] M. A. van Eijkelenborg, M. P. van Exter, and J. P. Woerdman, Phys. Rev. A **57**, 571 (1998).
[15] R. G. Harrison and D. J. Biswas, Phys. Rev. Lett. **55**, 63 (1985).
[16] C. O. Weiss, N. B. Abraham, and U. Hübner, Phys. Rev. Lett. **61**, 1587 (1988).
[17] J. H. Shirley, Am. J. Phys. **36**, 949 (1968).
[18] M. I. Kolobov, L. Davidovich, E. Giacobino, and C. Fabre, Phys. Rev. A **47**, 1431 (1993).
[19] H. Haken, Phys. Lett. **53A**, 77 (1975).
[20] D. Meiser and M. J. Holland, Phys. Rev. A **81**, 063827 (2010).
[21] Z. Chen, J. G. Bohnet, S. R. Sankar, J. Dai, and J. K. Thompson, Phys. Rev. Lett. **106**, 133601 (2011).
[22] Z. Chen, J. G. Bohnet, J. M. Weiner, K. C. Cox, and J. K. Thompson, arXiv:1211.0723.
[23] H. Statz, G. A. DeMars, D. T. Wilson, and C. L. Tang, J. Appl. Phys. **36**, 1510 (1965).
[24] I. D. Leroux, M. H. Schleier-Smith, and V. Vuletić, Phys. Rev. Lett. **104**, 073602 (2010).
[25] T. J. Kippenberg and K. J. Vahala, Science **321**, 1172 (2008).
[26] L. Ju, D. G. Blair, C. Zhao, S. Gras, Z. Zhang, P. Barriga, H. Miao, Y. Fan, and L. Merrill, Classical Quantum Gravity **26**, 015002 (2009).
[27] H. Tanji-Suzuki, I. D. Leroux, M. H. Schleier-Smith, M. Cetina, A. T. Grier, J. Simon, and V. Vuletić, Adv. At. Mol. Opt. Phys. **60**, 201 (2011).
[28] See Supplemental Material at http://link.aps.org/supplemental/10.1103/PhysRevLett.109.253602 for experimental and theoretical details.
[29] I. Teper, G. Vrijsen, J. Lee, and M. A. Kasevich, Phys. Rev. A **78**, 051803 (2008).
[30] M. H. Schleier-Smith, I. D. Leroux, and V. Vuletić, Phys. Rev. Lett. **104**, 073604 (2010).
[31] Z. Chen, J. G. Bohnet, J. M. Weiner, and J. K. Thompson, Rev. Sci. Instrum. **83**, 044701 (2012).
[32] J. K. Wahlstrand, J. T. Willits, T. R. Schibli, C. R. Menyuk, and S. T. Cundiff, Opt. Lett. **32**, 3426 (2007).
[33] D. Meiser and M. J. Holland, Phys. Rev. A **81**, 033847 (2010).
[34] A. E. Siegman, *Lasers* (University Science Books, Sausalito, CA, 1986), 1st ed.
[35] A. Lambrecht, J. M. Courty, S. Reynaud, and E. Giacobino, Appl. Phys. B **60**, 129 (1995).